Program Digest, 2019 IEEE International Ultrasonics Symposium (IUS)
Glasgow, Scotland, October 6-9, 2019

Validation of normalized singular spectrum area as a classifier for targeted microbubble enhancement

Elizabeth B. Herbst[1], Shiying Wang[1], Alexander L. Klibanov[1, 2], F. William Mauldin Jr. [1], John A. Hossack[1]

[1]Department of Biomedical Engineering [2]Division of Cardiovascular Medicine, University of Virginia, Charlottesville, VA 22908, USA

jh7fj@virginia.edu

Abstract – **Molecularly targeted microbubbles (MBs), comprising a gas core and a functionalized shell, 1-5 µm in diameter, enable visualization of disease marker concentration using a method termed ultrasound molecular imaging (USMI). The current state-of-the-art method for USMI based quantification of molecular markers is differential targeted enhancement (dTE), which employs destructive pulses of ultrasound to quantify the amount of targeted MB adherence. In this study, we sought to quantify the signal from adherent MBs non-destructively using a statistical parameter termed normalized singular spectrum area (NSSA) in a murine tumor model. The sensitivity and specificity of NSSA-based signal classification was compared to matched dTE measurements in a mouse hindlimb tumor.**

Keywords – ultrasound; molecular imaging; microbubbles; NSSA; singular value decomposition; differential targeted enhancement

I. Introduction

Ultrasound contrast agents, comprising highly echogenic microbubbles (MBs), are currently utilized for left ventricular opacification [1] and perfusion imaging [2], [3]. When conjugated with antibodies or peptides, MBs can be molecularly targeted to disease markers on the vascular endothelium, thus allowing for sensitive visualization of disease markers in a technique known as ultrasound molecular imaging (USMI). USMI has been utilized to detect vascular markers of cancer in numerous preclinical [4]–[7] and clinical [8]–[11] studies.

To differentiate between circulating "free" MBs and molecularly bound "adherent" MBs, most preclinical imaging protocols employ differential targeted enhancement (dTE) [12]–[20]. dTE is a measurement of the difference between the late enhancement ultrasound signal (circulating MBs + adherent MBs) and the signal after destruction of contrast through high-intensity ultrasound (circulating MBs only). Because dTE techniques extract a single image from the entire time course of injection, dTE is not real-time and typically requires wait times of 5-10 minutes before quantification [12], [13], [15], [21], [22]. While some clinical studies have quantified MB adherence through the late enhancement signal only [11], this method takes up to 30 min and requires manual delineation of the intratumoral region of interest (ROI) to eliminate false positive artifacts from strongly reflecting tissues [11], [23], [24].

Previous studies have shown that normalized singular spectrum area (NSSA), a statistical property of spatiotemporal data that is monotonic with interframe signal decorrelation, can differentiate between adherent and non-adherent MB signals in large vessel environments *in vitro* [25], [26]. In this study, we hypothesized that the NSSA values of adherent MB signals are statistically different from NSSA values of non-adherent MBs. This hypothesis was tested in a murine tumor model *in vivo*, and NSSA measurements were compared to corresponding dTE measurements. The classification performance of both techniques was assessed using receiver operating characteristic (ROC) analysis.

II. Materials and Methods

Microbubble fabrication

The method for MB preparation has been described previously [27]. Briefly, MBs were fabricated by sonicating a lipid micellar mixture of distearoyl phosphatidylcholine (Avanti Polar Lipids, Alabaster, AL, USA), polyethylene glycol stearate (Stepan Kessco, Elwood, IL, USA), and biotin-PEG3400-distearoylphosphatidylethanolamine (PEG_DSPE, Shearwater Polymers, Huntsville, AL, USA) and decafluorobutane gas (F2 Chemicals, Lancashire, UK) in normal saline. MBs were counted using a Coulter Multisizer 3 (Beckman Coulter, Brea, USA) and a streptavidin linker (Anaspec Inc, Fremont, CA, USA) was added at a concentration of 3 µg/10×10^6 MBs [28].

MBs were either conjugated to anti-mouse vascular endothelial growth factor receptor 2 (VEGFR2) antibody (clone Avas 12 a1, eBioscience, San Diego, CA, USA) or isotype control antibody (clone R35-95, BD Pharmingen, San Diego, CA, USA). MBs were conjugated to antibodies and MB size distribution and concentration was measured using a Coulter Multisizer 3 within 48 hours before each experiment.

Mouse hindlimb tumor model

Following an institutionally approved Animal Care and Use Committee Protocol, female C57 BL/6 mice were implanted with subcutaneous murine colon adenocarcinoma cells (MC38, Kerafast, Boston, MA, USA). When implanted tumors reached approximately 1 cm in diameter, mice were anesthetized with isoflurane gas (Henry Schein, Dublin, OH, USA) and imaged using a Verasonics programmable scanner (Vantage 256; Verasonics, Redmond, WA, USA). Doses of 2×10^7 MBs were diluted in 50 µL of phosphate-buffered saline and administered via tail vein catheter.

Each mouse received two injections of either VEGFR2-targeted or isotype control MBs. For one injection, MBs were destroyed at 1 min post-injection. For the other injection, MBs were destroyed at 6 min post-injection. For each of these experiments, dTE was measured by subtracting the mean post-burst signal from the mean pre-burst signal. The ordering of injections was randomized between individual mice.

Imaging and data collection

A Verasonics ultrasound scanner and 128-element L12-5 38 mm linear array transducer (Philips Healthcare, Andover, MA, USA) was used to implement pulse inversion imaging with synthetic aperture virtual source elements [7], [29], [30].

For dTE measurements, an intratumoral region of interest (ROI) of each mouse tumor was manually delineated. Mean signal within this ROI was calculated pre- and post-destruction. Corresponding NSSA values were calculated within this ROI from pre-destruction ultrasound signals. Each NSSA value was calculated from a sliding 3D window of spatiotemporal signals which was 5×5×25 samples, or 0.5mm×1mm×1.2s in the axial, lateral, and temporal dimensions, respectively. By sliding the window (step size = 1) axially and laterally, a complete mapping of NSSA values could be created for a 25-frame ensemble of ultrasound IQ data.

Data analysis

For a sample size of 9 mice, mean dTE and NSSA values were collected for highly reflective tissue signals, targeted MB signals, and non-targeted MB signals at each time point. A one-way analysis of variance (ANOVA) and *post-hoc* multiple comparisons test (significance level = 0.01) were used to compare these signals. The linear correlation was measured between dTE measurements and NSSA measurements for all MB signals.

The signal classification performance of dTE and NSSA was assessed using receiver operating characteristic (ROC) analysis. Classification performance was assessed for separation of tissue signals from all MB signals and separation of adherent MB signals (targeted, 6 min post-injection) and non-adherent MB signals (non-targeted, 6 min post-injection). Differences between the ROC area under the curve (AUC) were assessed using a one-tailed Henley and McNeil method [31] (significance level = 0.01).

III. Results and Discussion

Linear relationship between NSSA and dTE

For all MB signals, NSSA values had a strong linear correlation with dTE values, with an R^2 value of 0.82 (Fig. 1). These results suggest that NSSA measurements of MB adherence are consistent with the "state of the art" method for quantifying targeted MB adherence.

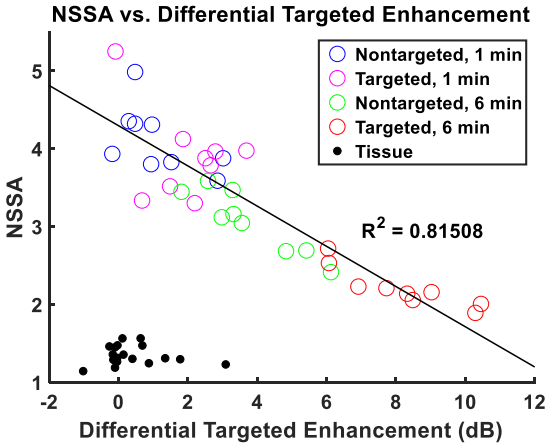

Fig. 1. NSSA measurements show a strong linear correlation with dTE measurements. NSSA and dTE measurements of tissue signals (black dots) also show that NSSA allows for robust separation of MB and tissue signals, while dTE is incapable of separating tissue signals from all MB signals.

ROC analysis of classification performance

For separation of all MB signals from tissue signals, ROC analysis (Fig. 2) revealed an AUC of 0.88 for dTE and 1.0 for NSSA. A one-tailed Hanley and McNeil test showed that NSSA-based classification was significantly more specific than dTE-based classification ($p<0.01$). For separation of adherent and non-adherent MB signals, ROC analysis yielded an AUC of 0.99 for dTE and 0.96 for NSSA. The Hanley and McNeil test showed that these two classification performances were not statistically significant ($p = 0.306$). These results suggest that for separation of tissue, adherent MB, and non-adherent MB

signals, NSSA matches or improves upon the signal classification performance of dTE.

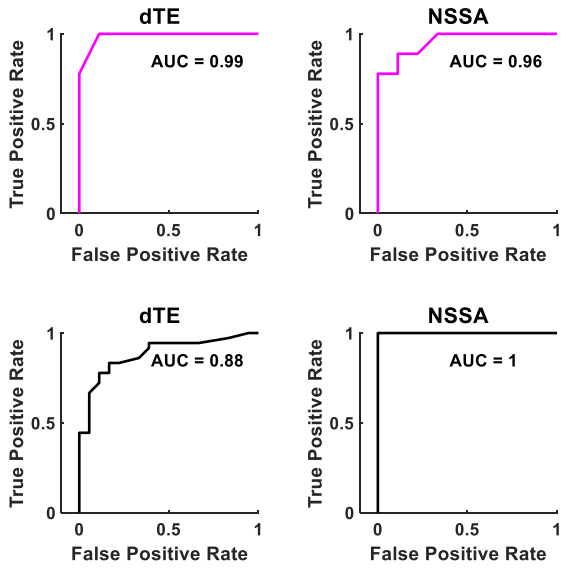

Fig. 2. NSSA matches the signal classification performance of dTE. For separation of adherent and non-adherent MBs (magenta plots), no statistically significant difference was found between NSSA and dTE based signal classification. For separation of tissue signals from MB signals (black plots), NSSA outperformed dTE with a ROC AUC of 1, equivalent to "ideal" classification performance.

IV. Conclusions

This study validated NSSA as a non-destructive measurement of MB adhesion in a murine tumor. NSSA matched or exceeded the MB classification performance of dTE without requiring destruction of contrast agent. The ability of NSSA to robustly separate between tissue signals, adherent MB signals, and non-adherent MB signals creates the potential for automatic segmentation of MB signals through NSSA-based image filtering.

References

[1] N. S. Chahal and R. Senior, "Clinical Applications of Left Ventricular Opacification," *JACC Cardiovasc. Imaging*, vol. 3, no. 2, pp. 188–196, 2010.

[2] V. Cantisani *et al.*, "Growing indications for CEUS: The kidney, testis, lymph nodes, thyroid, prostate, and small bowel," *Eur. J. Radiol.*, 2015.

[3] X. Wang, Z. Yu, R. Guo, H. Yin, and X. Hu, "Assessment of postoperative perfusion with contrast-enhanced ultrasonography in kidney transplantation," *Int. J. Clin. Exp. Med.*, 2015.

[4] S. V Bachawal *et al.*, "Earlier detection of breast cancer with ultrasound molecular imaging in a transgenic mouse model.," *Cancer Res.*, vol. 73, no. 6, pp. 1689–1698, 2013.

[5] A. Barua *et al.*, "Enhancement of ovarian tumor detection with alphavbeta3 integrin-targeted ultrasound molecular imaging agent in laying hens: a preclinical model of spontaneous ovarian cancer.," *Int. J. Gynecol. Cancer*, vol. 24, no. 1, pp. 19–28, Jan. 2014.

[6] T. Fischer *et al.*, "Vascular endothelial growth factor receptor 2-specific microbubbles for molecular ultrasound detection of prostate cancer in a rat model.," *Invest. Radiol.*, vol. 45, no. 10, pp. 675–684, 2010.

[7] S. Wang, E. B. Herbst, F. W. J. Mauldin, G. B. Diakova, A. L. Klibanov, and J. A. Hossack, "Ultra-low-dose ultrasound molecular imaging for the detection of angiogenesis in a mouse murine tumor model: How little can we see?," *Invest. Radiol.*, vol. 51, no. 12, pp. 758–766, 2016.

[8] G. Dimcevski *et al.*, "A human clinical trial using ultrasound and microbubbles to enhance gemcitabine treatment of inoperable pancreatic cancer," *J. Control. Release*, 2016.

[9] P. L. Khong, M. T. Chau, S. T. Fan, and L. L. Leong, "Ultrasound contrast agent Levovist in colour Doppler sonography of hepatocellular carcinoma in Chinese patients," *Australas Radiol*, vol. 43, no. 2, pp. 156–159, 1999.

[10] M. Smeenge *et al.*, "First-in-Human Ultrasound Molecular Imaging With a VEGFR2-Specific Ultrasound Molecular Contrast Agent (BR55) in Prostate Cancer: A Safety and Feasibility Pilot Study.," *Invest. Radiol.*, vol. 52, no. 7, pp. 419–427, 2017.

[11] J. K. Willmann *et al.*, "Ultrasound Molecular Imaging With BR55 in Patients With Breast and Ovarian Lesions: First-in-Human Results.," *J. Clin. Oncol.*, vol. 35, no. 19, pp. 2133–2140, 2017.

[12] C. R. Anderson *et al.*, "Ultrasound molecular imaging of tumor angiogenesis with an integrin targeted microbubble contrast agent.," *Invest. Radiol.*, vol. 46, no. 4, pp. 215–224, Apr. 2011.

[13] J. Bzyl *et al.*, "Molecular and functional ultrasound imaging in differently aggressive breast cancer xenografts using two novel ultrasound contrast agents (BR55 and BR38).," *Eur. Radiol.*, vol. 21, no. 9, pp. 1988–1995, 2011.

[14] N. Deshpande, Y. Ren, K. Foygel, J. Rosenberg, and J. K. Willmann, "Tumor angiogenic marker expression levels during tumor growth: longitudinal assessment with molecularly targeted microbubbles and US imaging.," *Radiology*, vol. 258, no. 3, pp. 804–811, Mar. 2011.

[15] D. B. Ellegala *et al.*, "Imaging tumor angiogenesis with contrast ultrasound and microbubbles targeted to alpha(v)beta3.," *Circulation*, vol. 108, no. 3, pp. 336–341, Jul. 2003.

[16] D. J. Lee, A. Lyshchik, and J. Huamani, "Relationship between retention of a vascular endothelial growth factor receptor 2 (VEGFR2)-targeted ultrasonographic contrast agent and the level of VEGFR2 expression in an in vivo breast cancer model.," *J. Ultrasound Med.*, vol. 2, pp. 855–866, 2008.

[17] M. A. Pysz *et al.*, "Vascular endothelial growth factor receptor type 2-targeted contrast-enhanced US of pancreatic cancer neovasculature in a genetically engineered mouse model: potential for earlier detection.," *Radiology*, vol. 274, no. 3, pp. 790–799, 2015.

[18] J. J. Rychak *et al.*, "Microultrasound molecular imaging of vascular endothelial growth factor receptor 2 in a mouse model of tumor angiogenesis," *Mol. Imaging*, vol. 6, no. 5, pp. 289–296, 2007.

[19] S. Turco, A. El Kaffas, J. Zhou, H. Wijkstra, J. K. Willmann, and M. Mischi, "Quantitative ultrasound molecular imaging for antiangiogenic therapy monitoring," in *IEEE International Ultrasonics Symposium, IUS*, 2016, vol. 2016-Novem.

[20] J. K. Willmann *et al.*, "US imaging of tumor angiogenesis with microbubbles targeted to vascular endothelial growth factor receptor type 2 in mice.," *Radiology*, vol. 246, no. 2, pp. 508–518, 2008.

[21] N. de Jong, P. J. . Frinking, A. Bouakaz, and F. J. Ten Cate, "Detection procedures of ultrasound contrast agents," *Ultrasonics*, vol. 38, no. 1–8, pp. 87–92, 2000.

[22] P. J. A. Frinking *et al.*, "Effects of acoustic radiation force on the binding efficiency of BR55, a VEGFR2-specific ultrasound contrast agent.," *Ultrasound Med. Biol.*, vol. 38, no. 8, pp. 1460–1469, Aug. 2012.

[23] M. X. Tang, N. Kamiyama, and R. J. Eckersley, "Effects of Nonlinear Propagation in Ultrasound Contrast Agent Imaging," *Ultrasound Med. Biol.*, 2010.

[24] M. X. Tang and R. J. Eckersley, "Nonlinear propagation of ultrasound through microbubble contrast agents and implications for imaging," *IEEE Trans. Ultrason. Ferroelectr. Freq. Control*, 2006.

[25] S. Wang, F. W. Mauldin Jr, and J. A. Hossack, "The physical source of adherent microbubble signal separation in singular spectrum-based targeted molecular imaging (SiSTM) of large vessels.," *IEEE Int. Ultrason. Symp.*, pp. 2153–2156, 2012.

[26] F. W. Mauldin Jr, D. Lin, and J. A. Hossack, "The singular value filter: a general filter design strategy for PCA-based signal separation in medical ultrasound imaging.," *IEEE Trans. Med. Imaging*, vol. 30, no. 11, pp. 1951–1964, 2011.

[27] A. L. Klibanov *et al.*, "Targeting and ultrasound imaging of microbubble-based contrast agents," in *Magnetic Resonance Materials in Physics, Biology and Medicine*, 1999.

[28] J. R. Lindner, J. Song, J. Christiansen, A. L. Klibanov, F. Xu, and K. Ley, "Ultrasound assessment of inflammation and renal tissue injury with microbubbles targeted to P-selectin.," *Circulation*, vol. 104, no. 17, pp. 2107–2112, 2001.

[29] E. B. Herbst, S. Unnikrishnan, S. Wang, A. L. Klibanov, J. A. Hossack, and F. W. Mauldin, "The Use of Acoustic Radiation Force Decorrelation-Weighted Pulse Inversion for Enhanced Ultrasound Contrast Imaging," *Invest. Radiol.*, vol. 52, no. 2, pp. 95–102, 2017.

[30] E. B. Herbst, S. Unnikrishnan, A. L. Klibanov, F. W. Mauldin, and J. A. Hossack, "Validation of Normalized Singular Spectrum Area as a Classifier for Molecularly Targeted Microbubble Adherence," *Ultrasound Med. Biol.*, 2019.

[31] J. A. Hanley and B. J. McNeil, "A method of comparing the areas under receiver operating characteristic curves derived from the same cases.," *Radiology*, 1983.